



Direct electrolytic separation of tungsten and cobalt from waste cemented carbide and electrochemical behavior of tungsten and cobalt ions in NaF–KF molten salts

Ming Li^{a,b}, Xiaoli Xi^{a,b,*}, Qingqing Liu^b, Zuoren Nie^{a,b}, Liwen Ma^{a,b}

^a National Engineering Laboratory for Industrial Big-data Application Technology, Beijing University of Technology, Beijing 100124, PR China

^b College of Material Science and Engineering, Key Laboratory of Advanced Functional Materials, Education Ministry of China, Beijing University of Technology, Beijing 100124, PR China

ARTICLE INFO

Keywords:

WC–10Co scrap
Electrolytic separation
Electrochemical behavior
NaF–KF melts

ABSTRACT

In this study, WC–10Co cemented carbide scrap was used as a consumable anode to separate and prepare tungsten and cobalt powders in NaF–KF melts at 1073 K. The feasibility of direct electrochemical dissolution of WC main phase to produce metallic tungsten was analyzed by thermodynamic calculations and experimental verifications. Furthermore, a series of electrolysis experiments were performed under constant cell voltage for selective preparation of tungsten and cobalt powders. The results show that metal cobalt powder was obtained at ≤ 0.6 V whereas metal tungsten powder was produced between 0.6 V and 1.2 V. The analysis of cathode products using scanning electron microscopy (SEM), X-ray diffraction (XRD), and X-ray photoelectron spectroscopy (XPS) show that tungsten and cobalt powders can be prepared in NaF–KF melts. Finally, linear sweep voltammetry (LSV) and electrochemical impedance spectroscopy (EIS) were used to investigate the dissolution of WC–10Co anode. The electrochemical properties of tungsten and cobalt ions in NaF–KF melts were studied by cyclic voltammetry (CV) and square wave voltammetry (SWV). The results show that WC–10Co anode could be used to produce tungsten and cobalt powders and the electroreduction of tungsten and cobalt ions in NaF–KF melts was achieved through a one-step reaction involving the transfer of two electrons.

1. Introduction

Cemented carbide is a composite material and usually composed of tungsten monocarbide (WC) embedded within a Co binder. Cemented carbides have characteristic high strength and hardness with a moderate toughness, thus providing an optimal solution as tool and component for metal cutting, rock drilling and wear resistance applications [1]. They are widely used in the manufacturing, mining, construction, oil and gas sectors. Cemented carbide, typically containing 40–95% tungsten, is the most hard and important metal in the carbides [2]. Cemented carbides found to have superior qualities than other hard materials in certain high-tech tooling and engineering applications. All the super hard materials such as diamond, the hardest of all, cubic boron nitride (CBN), polycrystalline diamond (PCD), and ceramics (Al_2O_3 , SiC etc.) have very low toughness, hence they are prone to form brittle fracture [3]. On the other hand, cemented carbides have a unique combination of high hardness, good toughness. Thus, they

constitute the most versatile group of hard materials for engineering and tooling applications [4].

Tungsten has excellent physicochemical properties such as high melting point, high density, and good corrosion resistance [5,6]. Therefore, tungsten found to have a large number of diverse applications in aerospace, electronics, automobiles, and atomic energy industries [7]. It also plays an important role in China's national economy. There are limited global resources for tungsten, but its usage continued to increase annually. Since 80% of tungsten powder is used to prepare cemented carbide [8], an alternative way to overcome the shortage of tungsten resources would be recycling of waste cemented carbide. The tungsten content in spent cemented carbide ranges from 74% to 91% [9], allowing a facile recovery and an access to cheaper tungsten sources compared to ore products [10]. Additionally, it also alleviates the over exploitation of tungsten ore and solves the pollution problem from mining of tungsten ore, promoting the sustainable development and utilization of tungsten ore in China.

* Corresponding author at: National Engineering Laboratory for Industrial Big-data Application Technology, Beijing University of Technology, Beijing 100124, PR China.

E-mail address: xixiaoli@bjut.edu.cn (X. Xi).

<https://doi.org/10.1016/j.jelechem.2018.12.032>

Received 16 September 2018; Received in revised form 14 December 2018; Accepted 17 December 2018

Available online 19 December 2018

1572-6657/ © 2018 Elsevier B.V. All rights reserved.

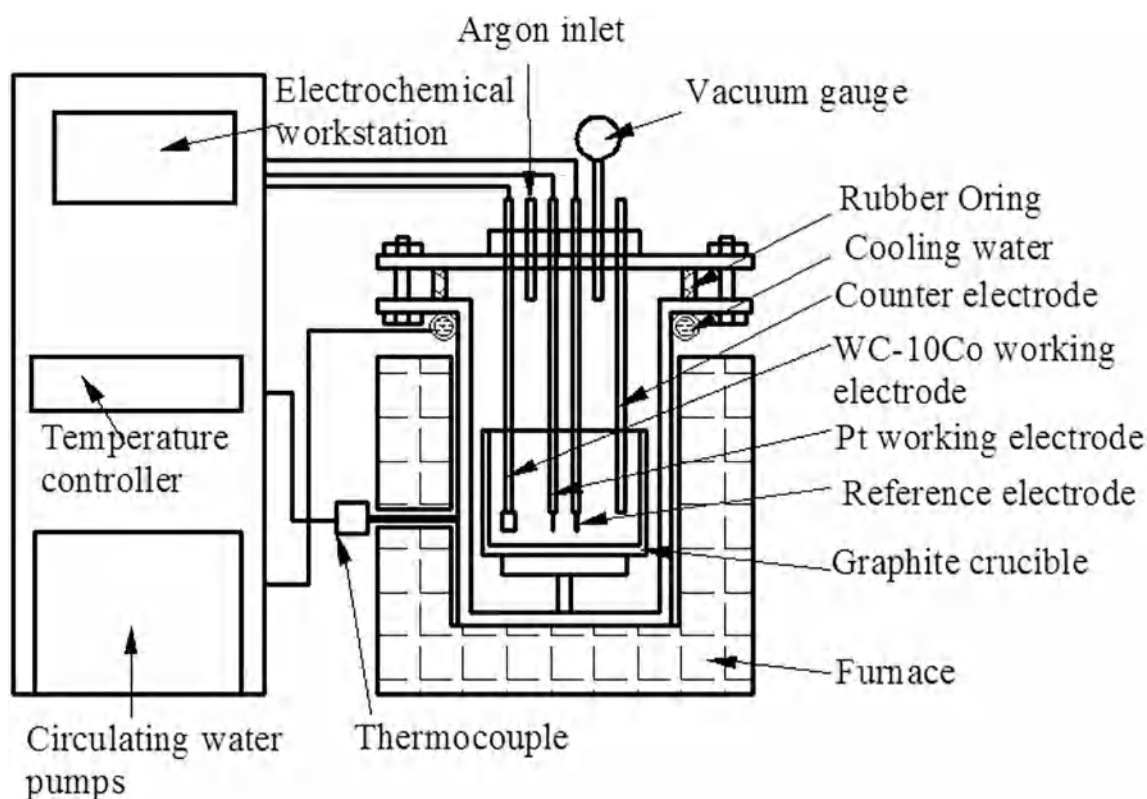


Fig. 1. Schematic diagram of electrolysis cell.

Table 1

The theoretical decomposition voltages of WC, NaF, and KF at 1073 K.

Reaction equation	ΔG_{1073K}° (KJ/mol)	E_{1073K}° (V)
$2\text{NaF}(l) = 2\text{Na}(l) + \text{F}_2(g)$	929.813	4.804
$2\text{KF}(l) = 2\text{K}(l) + \text{F}_2(g)$	919.908	4.763
$\text{WC}(s) = \text{W}(s) + \text{C}(s)$	35.699	0.185

Currently, various methods are available to recycle and recover waste cemented carbide. Mechanical crushing is a method that does not change the proportion of elements in the original cemented carbide [11]. In this method, the waste carbide was mechanically scrapped and then ball milled to obtain the same mixture as the waste carbide. Methods that can produce cobalt and tungsten carbide powders include acid leaching [12–14], zinc dissolution [15,16], high temperature treatment, and selective electrochemical dissolution [17,18]. These methods are based on characteristic properties of binder metal of cemented carbide such as low melting point and better chemical reactivity as compared to tungsten carbide. After dissolving cobalt of cemented carbide, cobalt powder is prepared through hydrometallurgy, the remaining tungsten carbide skeleton is mechanically crushed and ball milled to obtain the tungsten carbide powder. In general, nitrate stone melting and redox methods are used to produce cobalt and tungsten powders [19–21]. However, the saltpeter melting method involves the reaction of tungsten and sodium to produce sodium tungstate at high temperature, thus providing tungsten powder using tungsten smelting technology. On the other hand, the redox method involves oxidation of cemented carbide to corresponding oxides of tungsten carbide and cobalt, followed by crushing and ball milling, and finally, reduction of carbide provides both tungsten and cobalt powders [22].

The molten salt electrolysis technology has always been considered as an effective method for the preparation and recovery of metals with high melting points and corresponding alloys. Our group has innovatively combined molten salt electrolysis technology and waste

cemented carbide recovery technology to recover waste cemented carbide via a novel process called the molten salt electrochemical recovery method. In this method, the waste cemented carbide as a consumable anode and the chloride molten salt medium as an electrolyte are used. The different components of the cemented carbide are selectively dissolved by electrolysis in controlled conditions, and the cathode deposition is different. Compared to other conventional approaches, this method has several benefits such as simple and short recovery process, high purity, environmental benign, and regeneration of different metal components of waste cemented carbide. Xiaoli Xi and Guan hao Si [23,24] have successfully extracted tungsten from WC scrap via electrochemical extraction and investigated the electrochemical behavior of tungsten ion in blank NaCl–KCl melt at 1023 K. However, the recovery efficiency of tungsten powder is only 18%. Xiangjun Xiao et al. [25] successfully obtained tungsten and cobalt powders using molten salt electrolysis method and recovered waste cemented carbide in blank NaCl–KCl melt, thus leading to a short-process of regeneration of waste cemented carbide. However, electrochemical recovery of cemented carbide using NaF–KF has not been reported. NaF–KF has a relatively wide electrochemical window compared to NaCl–KCl. On the other hand, compared to the chloride molten salts, Hironori Nakajima et al. [26] reported that tungsten ions may form fluoro-tungsten complex ions in fluoride molten salts to promote the deposition of tungsten ions at the cathode.

In this study, waste WC–10Co cemented carbide was used as consumable anode to separate metallic tungsten and cobalt in NaF–KF molten salts at 1073 K. Based on the thermodynamic analysis, a series of electrolysis experiments were designed under constant cell voltage to prepare tungsten and cobalt powders in NaF–KF melts. XRD, SEM, and XPS were used to characterize the resulting cathode product. Several electrochemical techniques, such as linear sweep voltammetry, electrochemical impedance spectroscopy, cyclic voltammetry, and square wave voltammetry were used to investigate the electrochemical dissolution of waste WC–10Co cemented carbide and electrochemical

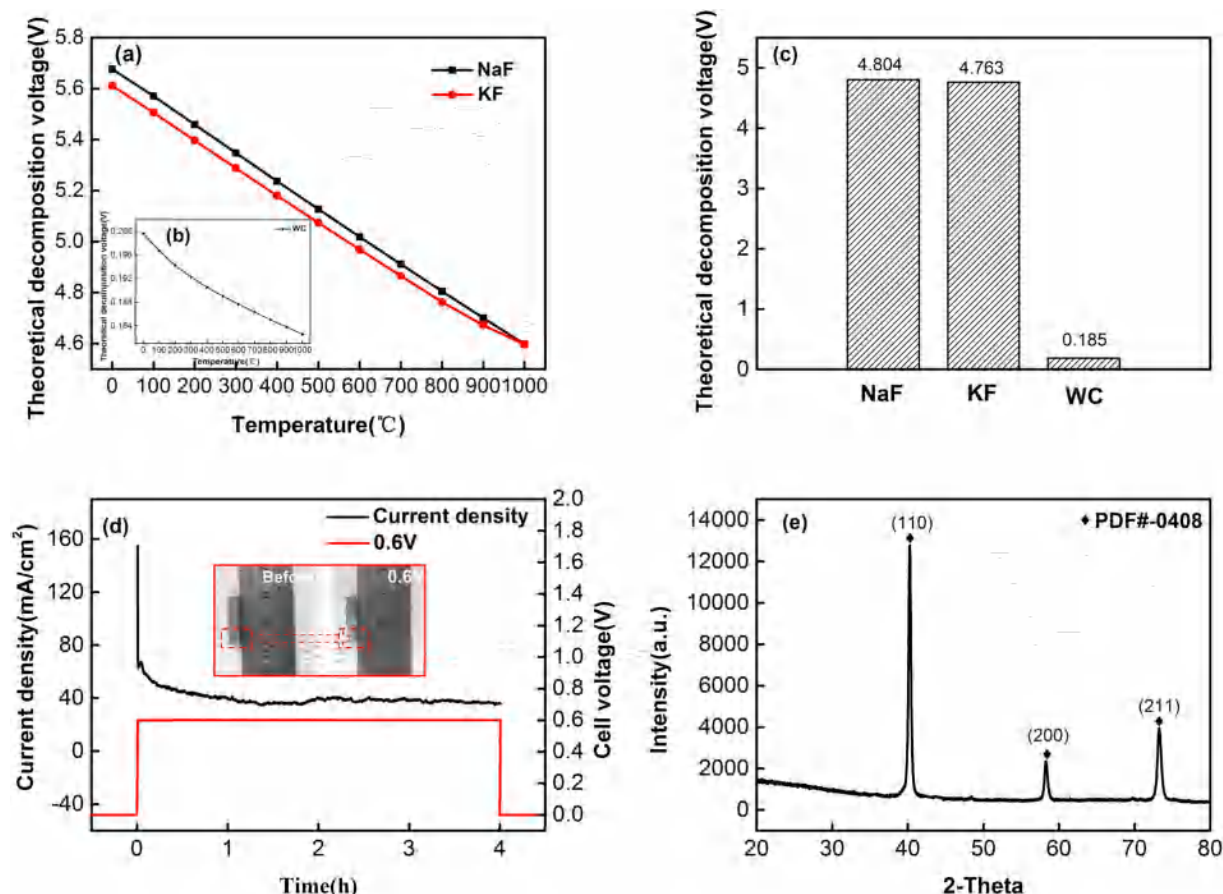


Fig. 2. (a) Theoretical decomposition voltages of NaF and KF versus temperature. (b) Theoretical decomposition voltages of WC versus temperature. (c) Theoretical decomposition voltage of NaF, KF, and WC at 1073 K. (d) Current density–time curve at 0.6 V and 1073 K for 4 h (area of WC electrode = 1.12 cm², inserted pictures: the photos of WC anode before and after electrolysis). (e) XRD pattern of cathode product at 0.6 V and 1073 K for 4 h.

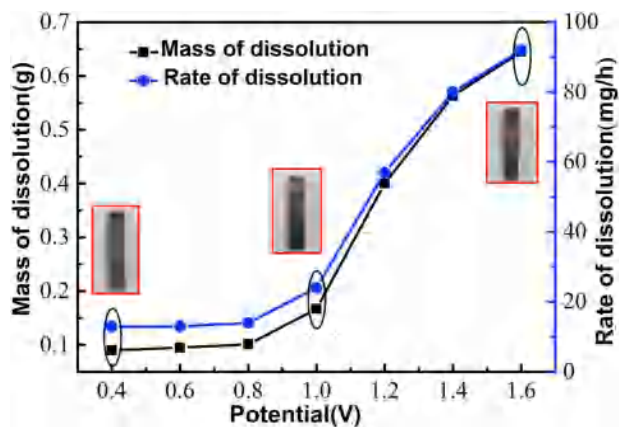


Fig. 3. The relationship between the mass of anode dissolution, rate of anode dissolution, and electrolysis voltages (inserted photos: the photographs of the anode after electrolysis at 0.4 V, 1.0 V, and 1.6 V).

behavior of the metal ions dissolved from the WC-10Co waste cemented carbide in the cathode.

2. Experimental

2.1. Electrochemical apparatus

Fig. 1 shows the apparatus used in the experiment. The apparatus is divided into four parts: a tubular resistance furnace, a temperature

control system, a cooling system, and an electrochemical measurement system. The temperature was controlled using a Pt-Rh thermocouple with an accuracy of ± 2 K. The circulating cooling system provides a stable temperature range for the electrolysis experiment, and the electrochemical measurement system was used to control and detect the electrochemical reaction.

2.2. Preparation and purification of the melts

The electrolytic bath consisted in a mixture of NaF:KF (Aladdin 98% and 99.5%, respectively) with the eutectic composition (NaF:KF = 39.7%:60.3%), which was introduced into a graphite crucible. The crucible was loaded into a furnace. After sealing the furnace, the temperature of the furnace was raised to 473 K for 2 h under vacuum and maintained at 473 K under vacuum for additional 24 h to remove the moisture. Subsequently, the mixture was heated to melt at 1073 K, where high purity argon gas (99.9%) was injected into the vessel to maintain an inert atmosphere.

2.3. Electrochemical test and characterization of cathode products

A two-electrode electrolysis system was employed for electrolysis of cemented carbide to obtain cobalt and tungsten powders. WC-10Co ($4 \times 4 \times 10$ mm) was used as a consumable anode and the total mass was 6.8 g, whereas nickel plate (8×20 mm) was used as a cathode. The cathode products obtained under different constant cell voltages were sonicated, washed with water, and dried at 40 °C for 24 h. Subsequently, the cathode products were characterized using X-ray diffraction (XRD, SHIMADZU, XRD-7000), field emission scanning

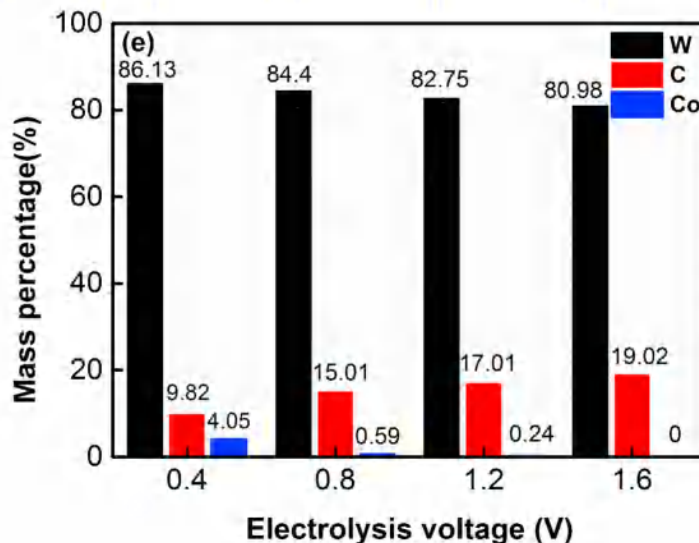
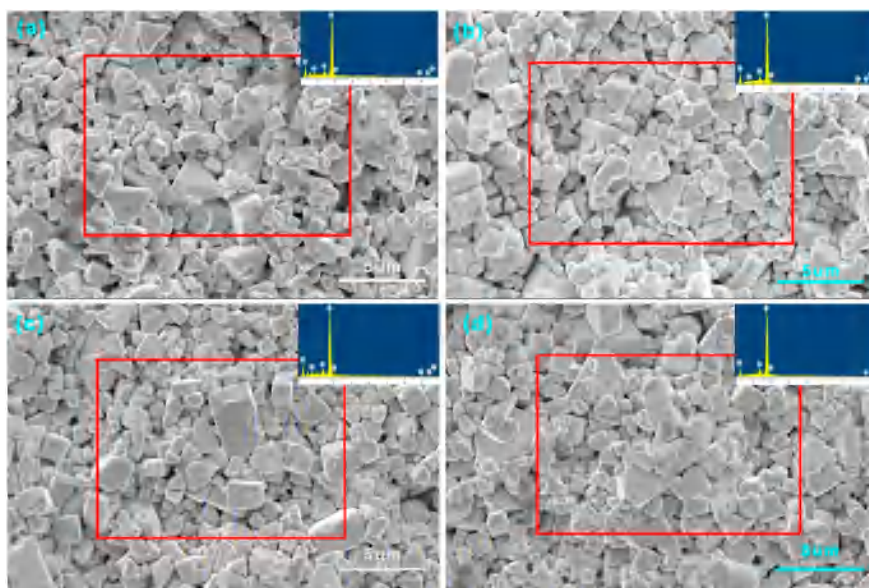


Fig. 4. SEM image and EDS analysis of WC-10Co cemented carbide after electrolysis (a) at 0.4 V, (b) at 0.8 V, (c) at 1.2 V, (d) at 1.6 V, (e) Histogram between the mass percentage of element and electrolysis voltage on the surface of WC-10Co cemented carbide.

electron microscopy (FESEM, JEOL, SU-8020) and X-ray photoelectron spectroscopy (XPS).

All electrochemical analysis was carried out on a PARSTAT 4000 electrochemical workstation with the Versa Studio software package (Advanced Measurement Technology, Inc., USA). A three-electrode system containing a platinum wire ($\phi 0.5$ mm), a graphite rod ($\phi 1$ mm), and waste WC-10Co was used as a working electrode. A platinum wire ($\phi 0.5$ mm) as a reference electrode, and a nickel rod ($\phi 3$ mm) as a counter electrode were used to investigate the electrochemical dissolution of waste WC-10Co cemented carbide. The lower end of the working electrode was thoroughly polished with SiC paper and then cleaned with ethanol in an ultrasonic bath. The active electrode surface was determined after each experiment by measuring the immersion depth of the electrode in the molten salt. The electrochemical behavior of metal ions dissolved from waste WC-10Co cemented carbide in the cathode was studied by linear sweep voltammetry, electrochemical impedance spectroscopy, cyclic voltammetry, and square wave voltammetry.

3. Results and discussion

3.1. Thermodynamic analysis and experimental verification of electrochemical dissolution of WC anode

Cemented carbide is a composite material prepared by sintering hard phase tungsten carbide and a small amount of binder phase metal cobalt. However, the electrochemical dissolution of the main phase tungsten carbide is the key step for electrochemical separation and preparation of metal tungsten and metal cobalt from the waste cemented carbide. Therefore, a thermodynamic calculation was used to analyze the direct electrochemical dissolution of WC main phase to give metallic tungsten. The electrochemical dissolution of the WC anode is a complex process, but the proposed strategy simplifies the entire electrochemical process by considering the three chemical reactions presented in Table 1. Theoretical decomposition voltages of WC, NaF, and KF occurred during the electrolysis process were calculated according to HSC Chemistry 6.0 and the results are shown in Fig. 2. The theoretical decomposition potential was calculated using Eq. (1):

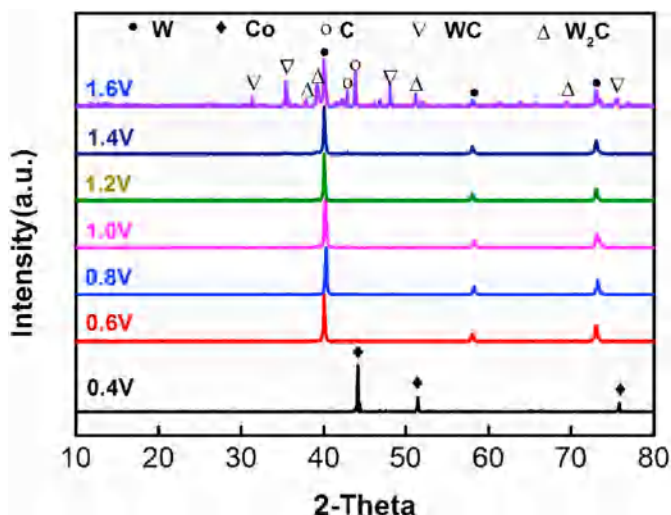


Fig. 5. XRD patterns of cathode products obtained at different electrolysis potentials at 1073 K for 7 h.

$$\Delta E_T^\theta = -\frac{\Delta G_T^\theta}{nF} \quad (1)$$

The variables were defined as following: ΔE_T^θ is the theoretical decomposition voltage, ΔG_T^θ is the standard Gibbs free energy, n is the number of electrons transferred, and F is the Faraday constant, which is 96,485 C/mol.

Fig. 2(a) and (b) shows the theoretical decomposition voltages at different temperatures. Notably, the theoretical decomposition voltages of NaF, KF, and WC gradually decreased as the temperature increased. Additionally, the electrolysis temperature for our experiment was 1073 K. Table 1 and Fig. 2(c) show the specific theoretical decomposition voltage value E_T^θ obtained at 1073 K. The theoretical decomposition voltages of WC and NaF were determined to be 0.185 V and 4.804 V at 1073 K, respectively, whereas the theoretical decomposition voltage of KF was found to be 4.763 V, which is less than that of NaF. Therefore, the theoretical range of the voltages from 0.185 V to 4.763 V was used during the electrolysis of WC anode. Further, the electrolytes NaF and KF are stable in this voltage range. Thermodynamically, the direct preparation of metallic tungsten from WC by molten salt electrolysis process is feasible in NaF–KF molten salts by controlling the cell voltage.

To verify the feasibility of direct electrochemical dissolution of WC main phase to produce metallic tungsten, an electrolysis experiment was carried out with 0.6 V at 1073 K for 4 h using tungsten carbide and nickel plate as anode and cathode, respectively. The current–time curve

and XRD pattern of the cathode product are shown in Fig. 2(d) and (e). As shown in Fig. 2(d), the current sharply increases to a peak level i.e. $\sim 160 \text{ mA/cm}^2$ and then decreases to the background level in the remaining period of electrolysis. The inserted pictures in Fig. 2(d) represent the anode before and after electrolysis, indicating a visible change in the shape during the electrolysis in NaF–KF melts at 1073 K. Fig. 2(e) shows the XRD pattern of cathode product, which has similar pattern as the body-centered cubic structure of standard tungsten, indicating electrochemical dissolution of WC main phase to produce metallic tungsten.

3.2. Electrolysis of WC–10Co cemented carbide anode

To explore the effect of electrolysis voltage on the anode dissolution and the cathode product formation, spent WC–10Co cemented carbide was selected as a consumable anode and a series of electrolysis experiments were designed with constant cell voltages. Different electrolysis voltages (0.4 V, 0.6 V, 0.8 V, 1.0 V, 1.2 V, and 1.4 V) were used for electrolysis. The inserted photographs in Fig. 3(a) show the anode after electrolysis with 0.4 V, 1.0 V, and 1.6 V, indicating a visible change in the shape with an increase in electrolysis voltages. This further supports that the anode is electrolyzed in NaF–KF melts at 1073 K. Furthermore, the anode plate was weighed before and after electrolysis to calculate the anode weight and volume loss and the rate of electrochemical dissolution is determined and calculated using the following equation (Eq. (2)) [27]:

$$r(\text{g} \times \text{h}^{-1}) = \frac{\Delta W}{t} \quad (2)$$

where r is the rate of dissolution ($\text{g} \times \text{h}^{-1}$); ΔW is the change in weight of the anode before and after electrolysis (g); t is the duration of electrolysis (h).

Fig. 3(a) shows the relationship between mass of anode dissolution, rate of anode dissolution, and electrolysis voltages. Evidently, the mass and rate of anode dissolution increase gradually at 0.4 V and 0.8 V, indicating only a small amount from the surface of the binder phase metallic cobalt of cemented carbide is dissolved and most of the main phase tungsten carbide remains undissolved. However, the mass and rate of anode dissolution rapidly increased at electrolysis voltages between 1.0 V and 1.6 V, indicating a large amount of the main phase tungsten carbide is dissolved.

In order to further investigate the WC–10Co anode dissolution, SEM and EDS were used to characterize the element distribution on the anode surface after electrolyzed with 0.4 V, 0.8 V, 1.2 V, and 1.8 V. Fig. 4 shows the micromorphology of WC–10Co anode surface after electrolysis. The compact surface of WC–10Co anode is broken into pieces and the change in micromorphology is small with the increase in

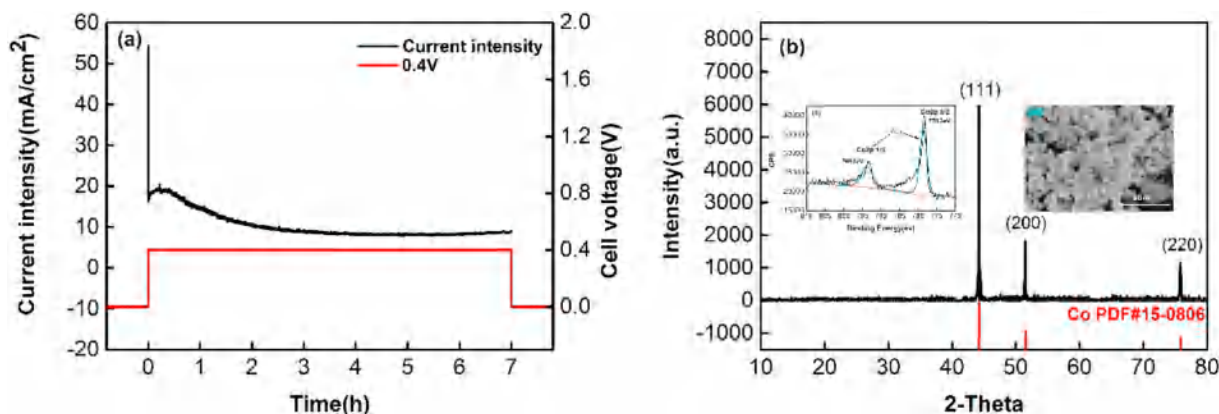


Fig. 6. (a) Current density–time curve at 0.4 V and 1073 K (area of WC–10Co electrode = 1.12 cm^2). (b) XRD pattern of the cathode product obtained at 0.4 V and 1073 K for 7 h. (c) XPS spectra of cathode product obtained at 0.4 V and 1073 K for 7 h. (d) SEM image of cathode product obtained at 0.4 V and 1073 K for 7 h.

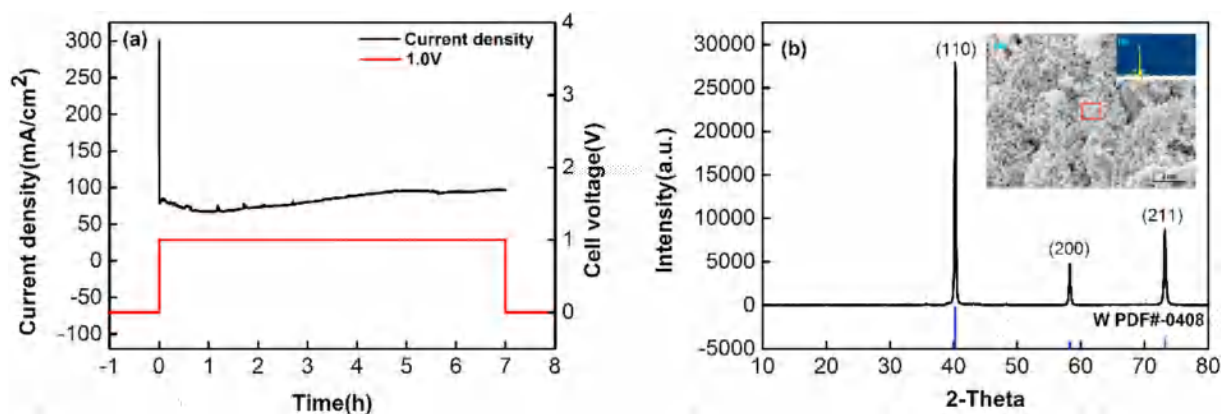


Fig. 7. (a) Current density–time curve at 1.0 V and 1073 K (area of WC–10Co electrode = 1.12 cm²). (b) XRD pattern of the cathode product obtained at 1.0 V and 1073 K for 7 h. (c) SEM image of cathode product obtained at 1.0 V and 1073 K for 7 h. (d) EDS spectra of cathode product obtained at 1.0 V and 1073 K for 7 h.

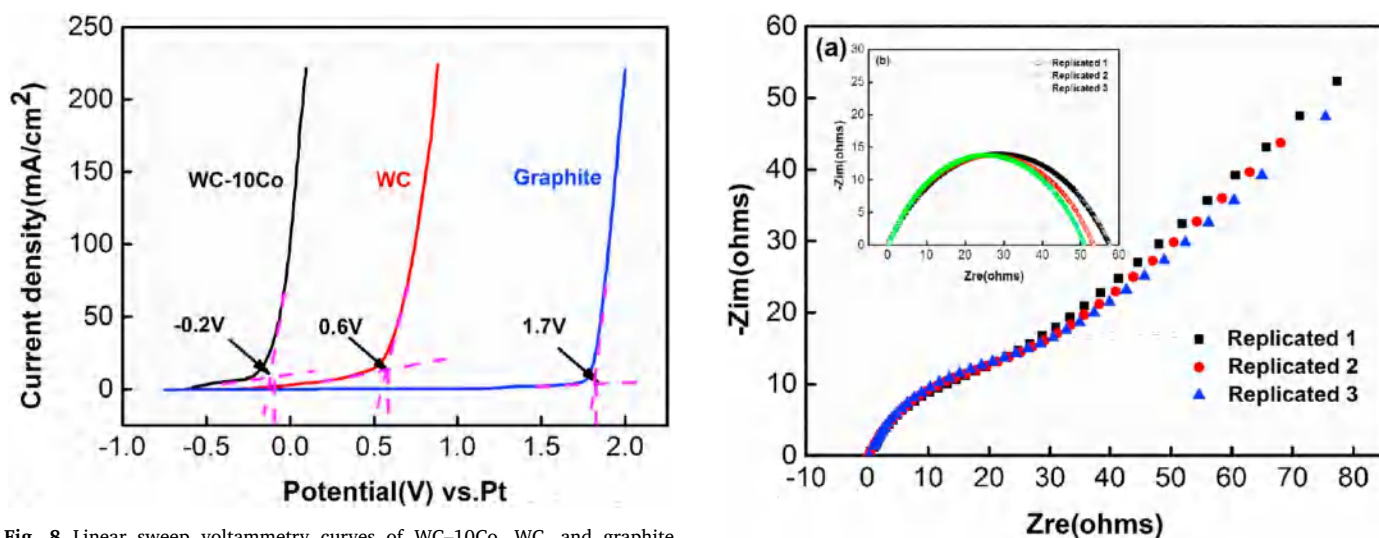


Fig. 8. Linear sweep voltammetry curves of WC–10Co, WC, and graphite electrodes.

electrolysis cell voltages. EDS was employed to investigate the influence of cell voltages on the different element dissolution of the anode surface. As shown in Fig. 4(e), the mass percentage of tungsten and cobalt gradually decreased and the mass of carbon increased, indicating tungsten carbide and binder cobalt are dissolved with the increase in electrolysis cell voltages. Compared with the dissolution of tungsten carbide, the binder phase cobalt on the surface of cemented carbide was completely dissolved at 1.6 V.

Additionally, the cathode products obtained at different electrolysis voltages were analyzed using XRD (Fig. 5). As shown in Fig. 5, the cathode product is metallic cobalt when electrolysis voltage is 0.4 V, whereas it is metallic tungsten between 0.6 V–1.4 V. When the electrolysis voltage is > 1.4 V, WC and W₂C appeared in the cathode product. These results indicate that the binder cobalt is first dissolved as cobalt ion and then cobalt ions are reduced to metal cobalt at low voltage. Further, tungsten carbide main phase also begins to dissolve with increasing electrolysis voltage. In the molten salt, both tungsten and cobalt ions are present. Since the amount of binder cobalt in cemented carbide is low, the concentration of the dissolved cobalt ions is also significantly low. Therefore, the precipitation of cobalt ions at the cathode is also low as compared to tungsten ions. On the other hand, potassium fluoride was favorable for tungsten ion deposition in the cathode [26]. Further, metallic tungsten can be obtained at high voltage. At high voltage, tungsten ions concentrate near the cathode and react with the carbon at the anode to form WC/W₂C.

Based on the results of cathode products at different electrolysis

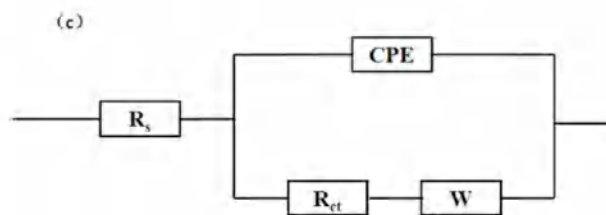


Fig. 9. (a) Complex impedance spectra of WC–10Co electrode in NaF–KF melt in the frequency range of 0.1–10 KHz at 1073 K. The applied potential was 0.4 V vs Pt. (b) Fitted data in the high-frequency region. (c) Corresponding equivalent circuit.

voltages, the optimal conditions for obtaining cobalt powder is 0.4 V for 7 h. Fig. 6(a) shows the curve of electrolysis current over time. When the electrolysis voltage is 0.4 V, the current intensity rapidly decreases and stabilizes at about 40 mA/cm² in a short time, which is attributed to a fact that the dissolution of binder metallic cobalt is slow at low current intensity. Fig. 6(b) represents the XRD analysis of the cathode product obtained at 0.4 V and 1073 K for 7 h. Notably, the diffraction peak of the product corresponds exactly to that of standard peak of metallic cobalt. Fig. 6(c) shows the XPS spectra of the cathode product formed at 0.4 V, the peaks of 2p 3/2 and 2p 1/2 at 778.3 eV and 793.3 eV, respectively, correspond to the peaks of metallic Co (0) [28]. Fig. 6(d) shows the SEM analysis of the obtained cobalt powder. The particle size of the cobalt powder was estimated to be ~1 μm with more

separated and uniform distribution of the crystallized particles. The conditions for obtaining tungsten powder are 1.0 V for 7 h. Fig. 7(a) shows the curve of electrolysis current intensity with time and the electrolysis voltage is 1.0 V, which indicates that the electrolysis process is not stable because of the dissolution of large amount of tungsten carbide main phase. Fig. 7(b) displays the XRD analysis of the product obtained under the electrolysis conditions. The diffraction peak of the product corresponds to the standard peak of metallic tungsten. Fig. 7(c) shows the SEM analysis of the product, revealing irregular shape of tungsten powder particles with a diameter of 200 nm. The EDS presented in Fig. 7(d), the cathode products were essentially composed of tungsten metals, confirming the formation of pure tungsten at the cathode.

3.3. Electrochemical analysis of WC-10Co anode dissolution

To investigate the dissolution potential of WC-10Co anode in NaF-KF molten salt, the polarization curves of WC-10Co, WC, and carbon rod were obtained with a scanning rate of 50 mV s^{-1} (Fig. 8). As shown in Fig. 8, the polarization curves of WC-10Co scrap, WC plate, and graphite rod rapidly increase at -0.2 V , 0.6 V , and 1.7 V , indicating the initial electrochemical dissolution potential of WC-10Co plate, WC plate, and graphite rod are -0.2 V , 0.6 V , and 1.7 V , respectively. It is obvious from comparison of the initial electrochemical dissolution potentials that WC-10Co anode is prone to electrochemical dissolution as compared to other anodes.

To understand the electrochemical oxidation resistance of WC-10Co cemented carbide, an electrochemical impedance spectroscopy (EIS) was used. Typically, three replicates of Nyquist plots were recorded for

WC-10Co anode in NaF-KF molten salt at a potential of 0.4 V (vs Pt) in the frequency range of 0.1 Hz to 10 KHz at 1073 K (Fig. 9(a)). A high-frequency semicircle was first observed followed by a straight line in the low-frequency region, indicating that the electrochemical dissolution process of the WC-10Co anode was controlled by combined charge transfer and diffusion phenomena in the solution. The high-frequency semicircle was attributed to the time constant of the charge transfer and double layer capacitance at the electrode-electrolyte interface. The intersections of semicircles with real axis give an estimate value of the resistance of solution (R_s) enclosed between the working and counter electrodes. The low-frequency liner portion is associated with Warburg type impedance related to the diffusion of soluble cobalt ions from the electrode to the bulk solution.

The complex impedance data were fitted according to the suitable equivalent circuits using the Zview fitting software and the results were presented in Fig. 9(c). In the circuit, R_s is the solution resistance, R_{ct} is the charge transfer resistance, and CPE is the constant phase element used to establish a more accurate fit due to the presence of capacitive loop that generates an irregular semicircle [29]. The dashed line in Fig. 9(b) represents the best fit of the data, estimating the average charge transfer resistance (R_{ct}) of WC-10Co and found to be 53.73Ω .

3.4. Cyclic voltammetry (CV) of cobalt and tungsten ions in NaF-KF melts

The electrochemical behavior of dissolved tungsten and cobalt ions from WC-10Co anode was studied using cyclic voltammetry and the cyclic voltammograms are presented in Fig. 10. According to the results of the cathode product with different cell voltages, cobalt ions were dissolved from binder metallic cobalt at 0.4 V for 7 h. Fig. 10(a) shows

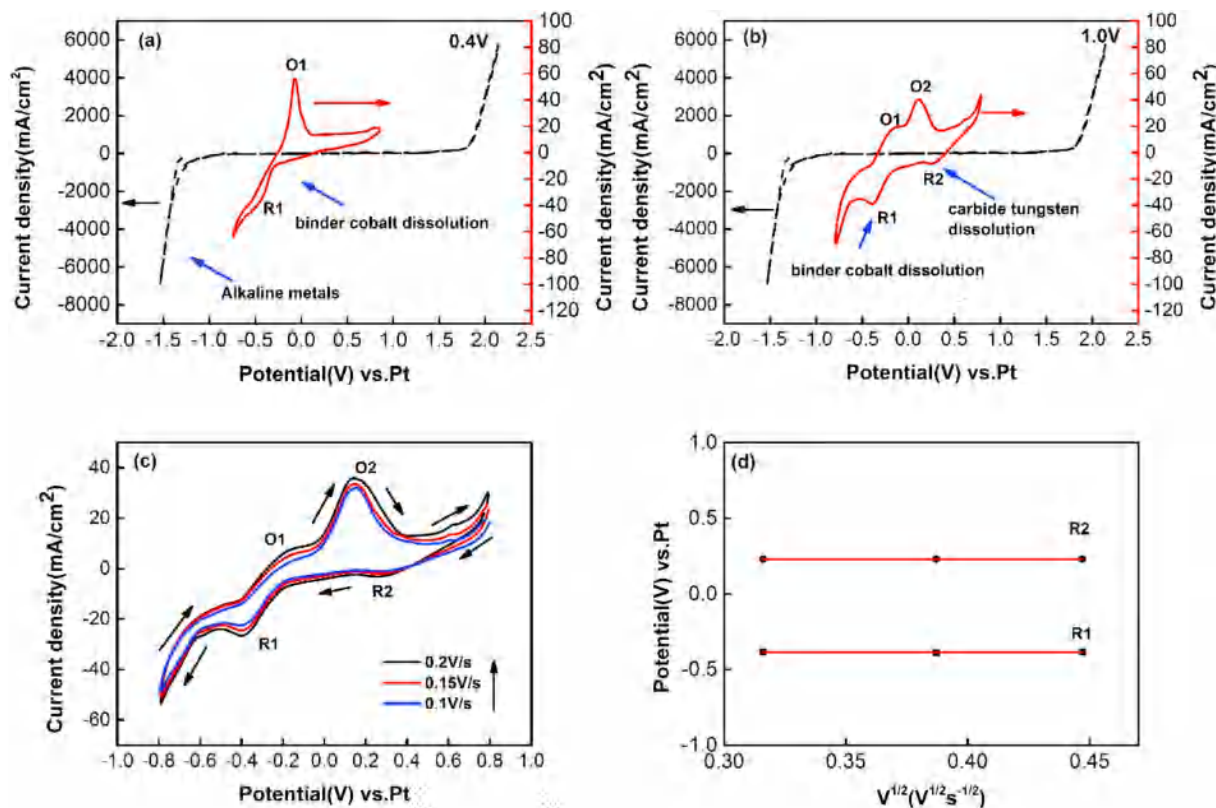


Fig. 10. (a) Cyclic voltammograms in the blank NaF-KF melt (dashed line: Pt electrode with 0.06 cm^2) and after completion of the WC-10Co cemented carbide electrolysis at 0.4 V (red line: Pt electrode with 0.06 cm^2). (b) Cyclic voltammograms in the blank NaF-KF melt (dash line: Pt electrode with 0.06 cm^2) and after completion of the WC-10Co cemented carbide electrolysis at 1.2 V (red line: Pt electrode with 0.06 cm^2). (c) Cyclic voltammograms obtained at various scan rates on a Pt electrode after electrolysis of WC-10Co cemented carbide in NaF-KF melt at 1073 K and 1.2 V (working electrode area: 0.06 cm^2). (d) Linear relationship of reduction peak potential versus square root of scan rate after electrolysis at 1.0 V . (For interpretation of the references to colour in this figure legend, the reader is referred to the web version of this article.)

the cyclic voltammogram in the blank NaF–KF eutectic melt before and after the WC–10Co electrolysis at 0.4 V and observed a sharp cathodic peak with cathodic return peak at -0.42 V and -0.13 V vs Pt, respectively. These redox waves correspond to the reduction of cobalt ions and dissolution of the deposited cobalt metal. The electroreduction of the cobalt ions proceeded with a one-step electrolysis process. Fig. 10(b) shows the cyclic voltammogram in the blank NaF–KF eutectic melt before and after the WC–10Co electrolysis at 1.0 V for 7 h and resulted a red curve with two pairs of redox peaks, a reduction peak potential of R1 at -0.38 V vs Pt and an oxidation peak potential O1 at -0.13 V vs Pt. Therefore, the reduction peak R1 and oxidation peak O1 on the left side in Fig. 10(b) correspond to the deposition and dissolution of cobalt metal, respectively. On the other hand, the reduction peak R2 and oxidation peak O2 on the right side in Fig. 10(b) represent deposition and dissolution of tungsten metal, respectively. Consequently, the precipitation of cobalt and tungsten ions are one-step reduction reactions.

Fig. 10(c) shows the cyclic voltammetry curves at different scanning rates of the cemented carbide electrolysis at 1073 K and 1.0 V for 7 h. Fig. 10(d) shows the relationship between the reduction peak potential and the square root of scan rate. In Fig. 10(c), significant reduction peaks at -0.38 V and 0.23 V correspond to the reduction peaks of cobalt and tungsten ions, respectively. As the scanning rate increases, the reduction peak current density also increases, whereas the potentials of reduction peak R1 and R2 do not have significant shift. Fig. 10(d) also shows that the potentials of reduction peak R1 and R2 remained nearly constant at -0.31 V vs Pt and 0.23 V vs Pt regardless of scan rates, indicating the reversibility of the reduction of cobalt and tungsten ions.

3.5. Square wave voltammetry (SWV) of cobalt and tungsten ions in NaF–KF melts

Square wave voltammetry was used to understand the electro-reduction behavior of cobalt and tungsten ions on the Pt wire electrode. Fig. 11(a) shows the square wave voltammetry curves at different frequencies during the electrolysis of WC–10Co cemented carbide at 1073 K and 0.4 V for 7 h, which presents a typical cobalt ion reduction wave recorded on a Pt wire at a potential of -0.42 V vs Pt.

The average number of exchanged electrons during the electrochemical reduction of cobalt ion can be calculated from the half width of the peak $W_{1/2}$, using Gaussian fit equation (Eq. (3)) [30]:

$$W_{1/2} = 3.52RT/nF \quad (3)$$

where n is the number of exchanged electrons, R is the ideal gas constant, T is the absolute temperature, and F is the Faraday constant.

The average number of electrons transferred was estimated at different frequencies of the square wave signal (Table 2). This indicates that the number of electrons transferred was close to 2, confirming that the reduction of cobalt ion occurred through a one-step, two-electron transfer reaction.

As shown in Fig. 11(b), Oster young and Barker [30,31] reported a relationship between height of the peak and square root of the frequency. The reversibility can be understood by plotting the maximum current densities of the current peak versus the square root of frequency of the square wave signal. A straight line was obtained, indicating the reduction of Co (II)/Co (0) is a diffusion-controlled process. Since the cathodic peak remained constant over a specific frequency range, the

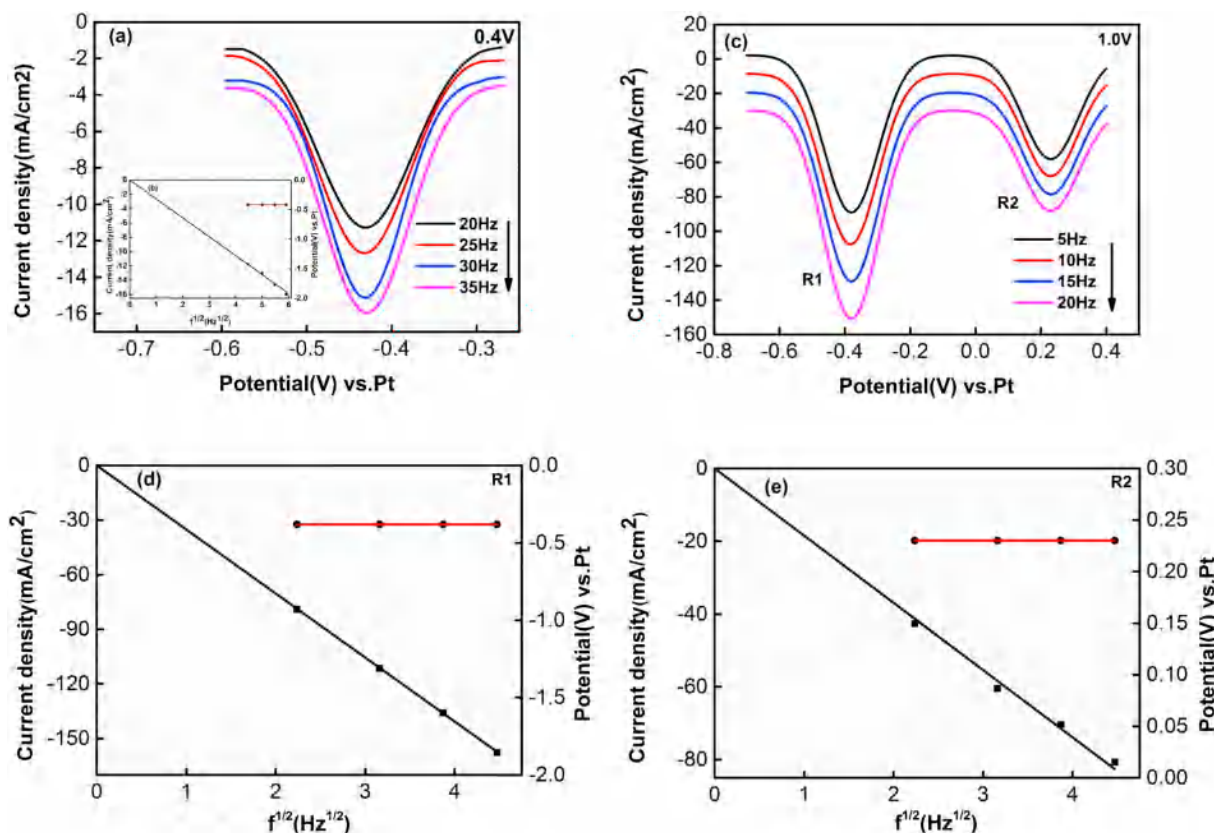


Fig. 11. (a) Square wave voltammograms of cobalt ion on a Pt electrode in NaF–KF melt at 1073 K after electrolysis at 0.4 V (Pt electrode with 0.06 cm^2). (b) Linear relationship of the cathodic peak current (black line) and reduction peak potential (red line) versus square root of frequency after electrolysis at 0.4 V. (c) Square wave voltammograms of cobalt and tungsten ions on a Pt electrode in NaF–KF melt at 1073 K after electrolysis at 1.0 V (Pt electrode with 0.06 cm^2). (d) Linear relationship of the cathodic peak current R1 (black line) and reduction peak potential (red line) versus square root of frequency after electrolysis at 1.0 V. (e) Linear relationship of the cathodic peak current R2 (black line) and reduction peak potential (red line) versus square root of frequency after electrolysis at 1.0 V. (For interpretation of the references to colour in this figure legend, the reader is referred to the web version of this article.)

Table 2

The values of $W_{1/2}$ and number of electrons (n) transferred in cobalt ions during electrolysis at 0.4 V.

Frequency	$W_{1/2}$	n
20 Hz	0.167	1.853
25 Hz	0.185	1.676
30 Hz	0.187	1.650
35 Hz	0.17233	1.799

Table 3

The values of $W_{1/2}$ and number of electrons (n) transferred in cobalt ions during electrolysis at 1.0 V.

Frequency	$W_{1/2}$	n
5 Hz	0.163	1.990
10 Hz	0.166	1.958
15 Hz	0.157	2.070
20 Hz	0.156	2.083

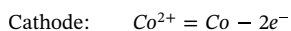
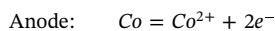
Table 4

The values of $W_{1/2}$ and number of electrons (n) transferred in tungsten ions during electrolysis at 1.0 V.

Frequency	$W_{1/2}$	n
5 Hz	0.161	2.019
10 Hz	0.164	1.982
15 Hz	0.162	2.006
20 Hz	0.167	1.946

reduction of cobalt ion is a reversible process (Fig. 11(b)), consistent with the results of the cyclic voltammetry.

Additionally, Fig. 11(c) shows the square voltammetry curves at different frequencies after the electrolysis of WC–10Co cemented carbide at 1073 K and 1.0 V for 7 h, two cathodic peaks appeared at -0.38 V vs Pt and -0.23 V vs Pt in the negative potential scan. The peaks of R1 and R2 correspond to the reduction peaks of cobalt and tungsten ions, respectively. Eq. (3) was used to calculate the average number of electrons exchanged during the electrochemical reduction of the cobalt and tungsten ions. It is evident from Tables 3 and 4, that two electrons were transferred in both cobalt and tungsten ions during the electroreduction process. Therefore, the reaction of cobalt at the anode and cathode is expressed by the following equations:



whereas the reaction of tungsten at the anode and cathode is expressed by the following equations:

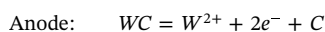


Fig. 11(d) and (e) indicates the relationship between maximum current densities of the current peak R1 and R2 versus the frequency square root of the square wave signal. The resulting straight lines confirm that the reductions of W (II)/W (0) and Co (II)/Co (0) were a diffusion-controlled process. Since the cathodic peaks R1 and R2 remained constant over a specific frequency range, the reduction of cobalt and tungsten ions is a reversible process. These results were also consistent with the cyclic voltammetry results.

4. Conclusions

Direct electrolytic separation of tungsten and cobalt from waste WC–10Co cemented carbide and the electrochemical behavior of tungsten and cobalt ions in NaF–KF molten salts at 1073 K were investigated. The electrochemical dissolution of WC main phase to produce metallic tungsten was validated by thermodynamic calculations and experimental verifications. Based on the thermodynamic analysis and electrolysis experiments of WC main phase, a series of constant cell voltage electrolysis experiments were performed to investigate selective preparation of tungsten and cobalt powders from waste WC–10Co cement carbide. It is evident from the results that cobalt powder with a diameter of 1 μm at ≤ 0.6 V and tungsten powder with a diameter of 200 nm at 1.0 V were obtained. Furthermore, the results of linear sweep voltammetry and electrochemical impedance spectroscopy confirm that waste WC–10Co cemented carbide can be used as a consumable anode for selective preparation of cobalt and tungsten powders. The cyclic voltammetry and square wave voltammetry show that electroreduction of the cobalt and tungsten ions occurred through a one-step process involving the two-electron transfer. The reduction process of these two ions was reversible and controlled by the diffusion in the melts.

Acknowledgments

This work was supported by National Natural Science Foundation of China (51621003, 51422401, and 51304010), National Key R&D Program of China (No. 2017YFB0305800), Science and Technology Project of Beijing Municipal Education Commission (KM201810005009), Beijing Municipal Natural Science Foundation (2172010) and the Construction Project for National Engineering Laboratory for Industrial Big-data Application Technology (312000522303).

References

- [1] A.K. Behnami, M. Sakaki, M.S. Bafghi, K. Yanagisawa, Facile microwave assisted fabrication of WC–Al₂O₃ composite powder from WO₃–Al–C mixture, *Chin. J. Nonferrous Met.* (12) (2017) 2630–2637, [https://doi.org/10.1016/S1003-6326\(17\)60291-7](https://doi.org/10.1016/S1003-6326(17)60291-7).
- [2] A. Shemi, A. Magumise, S. Ndlovu, N. Sacks, Recycling of tungsten carbide scrap metal: a review of recycling methods and future prospects, *Miner. Eng.* 122 (2018) 195–205, <https://doi.org/10.1016/j.mineng.2018.03.036>.
- [3] Sandvik, Carbide Recycling, <http://www.hyperion.sandvik.com/Documents/ProductLiterature/CarbideProducts/Recycling>, (2017) (Retrieved 15 September 2017).
- [4] Sandvik, Understanding Cemented Carbide, <http://www2.sandvik.com/>, (2016), Accessed date: 25 June 2016.
- [5] E. Lassner, W.D. Schubert, *Tungsten Properties, Chemistry, Technology of the Element, Alloys, and Chemical Compounds*, Kluwer Academic/Plenum Publishers, the United States, 1999, pp. 15–19.
- [6] V.K. Sarin, D. Mari, L. Llanes, *Comprehensive Hard Materials*, Elsevier: Ltd, Barcelona, 2014, pp. 23–24.
- [7] B. Yuan, L. Zhongshan, L. Liangxian, L. Qunyi, S. Linan, Z. Ming, Analysis of the tungsten resources reserve plan in China, *China Min. Mag.* 25 (2016) 15–18 <http://kns.cnki.net/kns/detail/detail.aspx?FileName=ZGKA201601005&DbName=CJFQ2016>.
- [8] Y.Z. Pan, J. Zhao, J. Zhang, Microstructure and tribological behavior of ultra-fine cemented carbides, *Key Eng. Mater.* 693 (2016) 586–593, <https://doi.org/10.4028/www.scientific.net/KEM.693.586>.
- [9] L. Luo, L. Kejun, A. Shibayama, Recovery of tungsten and vanadium from tungsten alloy scrap, *Hydrometallurgy* 72 (2004) 1–8, [https://doi.org/10.1016/S0304-386X\(03\)00121-X](https://doi.org/10.1016/S0304-386X(03)00121-X).
- [10] V.V. Malyshev, A.I. Gab, M.G. Escard, Molybdenum electrometallurgical processes in ionic melts, *Mater. Manuf. Process.* 23 (2008) 748–751, <https://doi.org/10.1080/10426910802381942>.
- [11] P. Priarone, M. Robiglio, L. Settineri, Milling of Austempered Ductile Iron (ADI) with recycled carbide tools, *Int. J. Adv. Manuf. Technol.* 82 (2015) 501–507, <https://doi.org/10.1007/s00170-015-7387-5>.
- [12] J. Lee, E. Kim, J. Kim, W. Kim, B.D. Pandey, Recycling of WC–Co hardmetal sludge by a new hydrometallurgical route, *Int. J. Refract. Met. Hard Mater.* 29 (2011) 365–371, <https://doi.org/10.1016/j.jrmhm.2011.01.003>.
- [13] C. Edtmaier, R. Schiesser, C. Meissl, Selective removal of the cobalt binder in WC/Co based hardmetal scraps by acetic acid leaching, *Hydrometallurgy* 76 (2005) 63–71, <https://doi.org/10.1016/j.hydromet.2004.09.002>.
- [14] T. Kojima, T. Shimizu, R. Sasai, Recycling process of WC–Co cermets by

- hydrothermal treatment, *J. Mater. Sci.* 40 (2005) 5167–5172, <https://doi.org/10.1007/s10853-005-4407-0>.
- [15] C.S. Freemantle, N. Sacks, M. Topic, C.A. Pineda-Vargas, PIXE characterization of byproducts resulting from the zinc recycling of industrial cemented carbides, *Nucl. Instrum. Methods Phys. Res., Sect. B* 363 (2015) 167–172, <https://doi.org/10.1016/j.nimb.2015.07.064>.
- [16] H.E. Hilliard, *Recycling Superalloy Scrap by Vapor Phase Zinc Embrittlement*. U.S. Patent, (1988).
- [17] B. Yang, G. Chen, A. Shi, B. Liu, Review on technologies of short recycle process for scrap cemented carbide, *Mater. Rev.* 29 (2015) 68–74 <http://kns.cnki.net/kns/detail/detail.aspx?FileName=CLDB201503014&DbName=CJFQ2015>.
- [18] S.S. Kamal, P.K. Sahoo, J. Vimala, B. Shanker, P. Ghosal, L. Durai, Synthesis of high purity tungsten nanoparticles from tungsten heavy alloy scrap by selective precipitation and reduction route, *J. Alloys Compd.* 678 (2016) 403–409, <https://doi.org/10.1016/j.jallcom.2016.03.303>.
- [19] J.C. Lin, J.Y. Lin, S.P. Jou, Selective dissolution of the cobalt binder from scraps of cemented tungsten carbide in acids containing additives, *Hydrometallurgy* 43 (1996) 47–61, [https://doi.org/10.1016/0304-386X\(96\)00023-0](https://doi.org/10.1016/0304-386X(96)00023-0).
- [20] Y. He, L. Chen, B. Huang, Recycling of heavy metal alloy turnings to powder by oxidation–reduction process, *Int. J. Refract. Met. Hard Mater.* 21 (2003) 227–231, [https://doi.org/10.1016/S0263-4368\(03\)00009-X](https://doi.org/10.1016/S0263-4368(03)00009-X).
- [21] B. Liu, A. Shi, A.Q. Su, Recovery of tungsten carbides to prepare the ultrafine WC-Co composite powder by two-step reduction process, *Powder Technol.* 306 (2016) 113–119, <https://doi.org/10.1016/j.powtec.2016.10.071>.
- [22] W.G. Jung, Recovery of tungsten carbide from hard material sludge by oxidation and carbothermal reduction process, *J. Ind. Eng. Chem.* 20 (2014) 2384–2388, <https://doi.org/10.1016/j.jiec.2013.10.017>.
- [23] G.H. Si, X.L. Xi, Z.R. Nie, L.W. Ma, Preparation and characterization of tungsten nanopowders from WC scrap in molten salts, *Int. J. Refract. Met. Hard Mater.* 54 (2016) 422–426, <https://doi.org/10.1016/j.ijrmhm.2015.10.002>.
- [24] X.L. Xi, G.H. Si, Z.R. Nie, L.W. Ma, Electrochemical behavior of tungsten ions from WC scrap dissolution in a chloride melt, *Electrochim. Acta* 184 (2015) 233–238, <https://doi.org/10.1016/j.electacta.2015.10.071>.
- [25] X.J. Xiao, X.L. Xi, G.H. Si, Z.R. Nie, L.W. Zhang, L.W. Ma, Direct electrochemical preparation of cobalt, tungsten, and tungsten carbide from cemented carbide scrap, *Metall. Mater. Trans. B Process Metall. Mater. Process. Sci.* 48 (2017) 692–700, <https://doi.org/10.1016/j.electacta.2015.10.071>.
- [26] K. Nitta, T. Nohira, R. Hagiwara, M. Majima, S. Inazawa, Electrodeposition of tungsten from ZnCl₂–NaCl–KCl–KF–WO₃ melt and investigation on tungsten species in the melt, *Electrochim. Acta* 55 (2010) 1278–1281, <https://doi.org/10.1016/j.electacta.2009.10.021>.
- [27] L.W. Hu, Y. Song, J.B. Ge, S. Jiao, J. Chen, Electrochemical metallurgy in CaCl₂–CaO melts on the basis of TiO₂–RuO₂ inert anode, *J. Electrochem. Soc.* 163 (2016) E33–E38, <https://doi.org/10.1149/2.0131603jes>.
- [28] National Institute of Standards and Technology, NIST X-ray Photoelectron Spectroscopy Database, https://srdata.nist.gov/xps/EngElmSrchquery.aspx?EType=PE&CSOpt=Retri_ex_dat&Elm=Co.
- [29] X. Wu, H. Ma, S. Chen, Z. Xu, A. Sui, General equivalent circuits for faradaic electrode processes under electrochemical reaction control, *J. Electrochem. Soc.* 146 (1999) 1847–1853, <https://doi.org/10.1149/1.1391854>.
- [30] J.J. O’Dea, J. Osteryoung, R.A. Osteryoung, Theory of square wave voltammetry for kinetic systems, *Anal. Chem.* 53 (1981) 695–701, <https://doi.org/10.1021/ac00227a028>.
- [31] L. Ramaley, M.S. Krause, Theory of square wave voltammetry, *Anal. Chem.* 41 (1969) 1362–1365.